Delft University of Technology

19.1 A 300MHz-BW, 27-to-38dBm In-Band OIP3 sub-7GHz Receiver for 5G Local Area Base Station Applications

Montazerolghaem, Mohammad Ali; De Vreede, Leo C.N.; Babaie, Masoud

Citation (APA)
Montazerolghaem, M. A., De Vreede, L. C. N., & Babaie, M. (2023). 19.1 A 300MHz-BW, 27-to-38dBm In-Band OIP3 sub-7GHz Receiver for 5G Local Area Base Station Applications. In *2023 IEEE International Solid-State Circuits Conference, ISSCC 2023* (pp. 292-294). (Digest of Technical Papers - IEEE International Solid-State Circuits Conference; Vol. 2023-February). Institute of Electrical and Electronics Engineers (IEEE). https://doi.org/10.1109/ISSCC42615.2023.10067266

Important note
To cite this publication, please use the final published version (if applicable).
Please check the document version above.

19.1 A 300MHz-BW, 27-to-38dBm In-Band OIP3 sub-7GHz Receiver for 5G Local Area Base Station Applications

Mohammad Ali Montazerolghaem, Leo C. N. de Vreede, Masoud Babaie

Delft University of Technology, Delft, The Netherlands

Recently, the so-called sub-6GHz band of the 5G new radio (NR) has been extended to 7.125GHz to address the relentless customer demand for higher data-rate communication. This demands a new design approach for the local area base-station (LA-BS) receivers (RXs) to cover a wide operating frequency range of 0.41 to 7.125GHz. Moreover, for NR bands above 3GHz, the maximum RF bandwidth (BW) is as high as 400MHz, in which a -35dBm modulated in-band (IB) blocker can be present. These impose stringent BW and IB linearity requirements for the baseband amplifiers in the LA-BS receivers. In addition to IB interferences, a -15dBm continuous-wave (CW) out-of-band (OOB) close-in blocker can also be present at 60MHz offset frequency from the passband edges, thus demanding a highly selective RX. Finally, the blocker 1dB compression point (B_{1dB}) becomes a key parameter for local area co-location applications in which the power of the far-out OOB blocker can be as large as -4dBm.

Prior art conventionally tried to address those challenges by choosing mixer-first architectures. However, if the TIA's input impedance is used to satisfy the input matching [1], the RX IB linearity will be limited by the signal swing at the TIA's input. Hence, [2] added a series resistor prior to the TIAs to provide the input matching, and improve the IB linearity by making the TIA's input a virtual ground. However, the series resistor degrades the RX noise figure (NF). Therefore, [3] added an auxiliary noise-canceling path to remove the matching resistor noise, at the cost of doubling the number of wideband TIAs and thus RX's power consumption (P_{DC}). Alternatively, as shown in Fig. 19.1.1, an LNTA with a band-stop N-path filter in its feedback can be adopted to improve the NF without sacrificing P_{DC}, and a translational feedback network can be used to provide the input matching [4]. However, the filtering order, IB linearity, and operating frequency of this structure are insufficient for LA-BS stringent requirements. To improve on those limitations, this paper, for the first time, presents a sub-7GHz RX capable of providing the linearity requirements of the local area base-station applications.

It is observed that the RX operating frequency is limited at the LNTA output by its output resistance (R_O) and total parasitic capacitance (C_{par}) of the node. Since a larger R_O is required to operate in the current mode and reduce the TIAs' noise contribution to NF, C_{par} must be minimized. In prior art, two sets of switches are used for signal downconversion and N-path filtering. Interestingly, the N-path filter switches connected to the LNTA's output can be removed, and the right plates of the notch filter capacitors can be connected to the outputs of the corresponding phase of the downconverter switches, as shown in Fig. 19.1.1-top. Consequently, C_{par} is reduced, extending the operating frequency to above 7GHz.

The baseband filter has three main tasks. First, it should offer a high-order lowpass transfer function to attenuate close-in blockers sufficiently. Second, its input impedance must be low enough to minimize the voltage swing at the LNTA output and TIA input to improve RX IB and OOB linearity. Third, its loop gain should be large enough to suppress the TIA nonlinear terms.

Figure 19.1.2 shows the schematics of the conventional single-pole TIA (SP-TIA) and Rauch filter adopted in the proposed RX. In both structures, R_F determines the transimpedance gain, and C_{IN} should be large enough to ensure that the major part of the OOB blocker current goes to ground. Otherwise, the last stage of the amplifier should sink/source that current and stay linear, thus demanding high P_{DC}. Even considering the same C_{IN} and R_F values for a fair comparison, the Rauch filter offers several benefits over the conventional single-pole TIA. First, it inherently exhibits second-order filtering, thus improving OOB linearity. Second, as shown in Fig. 19.1.2, the transfer function and maximum input impedance (Z_{IN}) of the Rauch filter are mainly determined by the passive components with a negligible effect from the OpAmp's unity-gain BW (ω_u). This is a great feature, especially for highly linear and large BW receivers, in which maintaining the OpAmp DC gain (A_0) and simultaneously increasing ω_u lead to high P_{DC} and stability issues. On the contrary, the SP-TIA in-band impedance is inversely proportional to the OpAmp open-loop gain (A), and consequently, an extremely large Z_{IN} peaking is inevitable even when $\omega_u=100\times\omega_{3-dB}$, where ω_{3-dB} is the desired 3dB BW. Third, the Rauch TIA offers a larger loop gain at the passband edge and transition band due to the presence of two complex-conjugate zeros at $1/\sqrt{(R_F R_1 C_F C_{IN})}$, as shown in Fig. 19.1.2. By properly choosing R_1, zeros can become smaller than ω_{3-dB}, and consequently compensate for TIA gain drop, improving IB and OOB linearity at the passband edge and transition band, respectively. Note that there is a tradeoff in choosing the R_1 value, as a larger R_1 increases the loop gain but, at the same time, leads to a higher Z_{IN} peak.

Figure 19.1.3 depicts the complete block diagram of the proposed RX. To improve the filtering order of the TIA, a third-order highpass filter, comprising two series capacitors

(C_H) and one shunt inductor (L_H), is placed in parallel with R_F. Ground ports of the inductors driven by complementary LOs are then connected to halve the number of baseband inductors. Each resulting inductor is then realized using a gyrator with a load capacitor (see Fig. 19.1.3 bottom right). Note that the gyrators' noise has a negligible contribution to the RX NF as it faces a highpass filter when traveling to the TIA output. Finally, a three-stage OpAmp is used as the TIA amplifier to ensure high loop gain for satisfying the IB linearity requirements of LA-BS applications. Miller and feed-forward compensation techniques are also used to stabilize the OpAmp and achieve enough phase margin. The first- and third-stage determine the OpAmp P_{DC}, as the former should satisfy the noise requirement, and the latter needs to stay linear while sinking/sourcing an IB blocker current.

To achieve a flat response within the channel BW, a second branch comprising a series capacitor (C_2) and a baseband amplifier with a gain of $-A_C$ is added in parallel with the main capacitor (C_1), as shown in Fig. 19.1.1-bottom. Here, the equivalent capacitance at the RX input is $C_{eq}=(C_1+C_2)-G_M Z_{IN}(A_C C_2-C_1)$, where G_M is the LNTA transconductance. Due to its bandpass characteristic, Z_{IN} reaches its maximum just below the passband edge. Hence, C_{eq} reduces at those frequencies, thus enhancing the BW and flattening the IB response. Outside the BW, Z_{IN} reduces over frequency, thus increasing C_{eq} and filtering roll-off. Note that both the noise and linearity requirements of the added amplifiers are relaxed since their input is connected to an almost virtual ground and their noise experiences a notch filter when appearing at the RX output.

The proposed RX is fabricated in 40nm CMOS technology and occupies an active area of 0.4mm² (Fig. 19.1.7). Figure 19.1.4 shows small- and large-signal measurement results. The S_{11} is <-10dB across the RX operating frequency of 0.4 to 7.3GHz. The RX gain (NF) is 38dB (3.2dB) at 1GHz LO frequency (f_{LO}) and reaches 35.7dB (5.8dB) at f_{LO}=7GHz. As shown in Fig. 19.1.4, the measured BW is disrupted by the TIA's impedance peaking when A_C is OFF. Turning ON the A_C and adjusting C_2 recovers the BW and the filtering order of the RX. Moreover, enabling the active inductors in Rauch TIAs improves the filtering order by 10dB/dec. The measured IB linearity is +38dBm at low IB frequencies, and reduces to +27dBm near ω_{3-dB}. The OOB linearity performance is also depicted in Fig. 19.1.4, in which the IIP2, IIP3, and B_{1dB} are respectively +67.7dBm, +11dBm, and -4.8 dBm at $\Delta f/\omega_{3-dB}$ =3, where Δf is a frequency offset from f_{LO}. The RX NF is only degraded by 5.5dB when facing a 0dBm CW blocker at $\Delta f/\omega_{3-dB}$=5 (see Fig. 19.1.4).

Figure 19.1.5 shows the EVM measurement results in different scenarios. Based on the 3GPP standard, the RX throughput must be >95% for reference sensitivity, in-band, close-in, and far-out blocking tests. In the reference sensitivity test, a 96% throughput is achieved when a 50MS/s -87.7dBm QPSK signal is applied to the RX. Then, the desired signal power is increased by 6dB for the blocking tests. Thanks to the RX high IB linearity, all symbols are appropriately received in the presence of a -35dBm 20MS/s modulated IB blocker. In the close-in blocking test, when facing a -15dBm CW close-in blocker at 60MHz offset from the BW edge, all desired symbols are received correctly due to the high-order filtering of the RX. Then, based on the co-location requirements, a -4dBm CW far-out blocker is applied to the RX, and a 100% throughput is achieved. Thus, the proposed RX satisfies all of the 3GPP requirements with enough margin. Finally, as depicted in Fig. 19.1.5-bottom, the RX performance is also tested with higher order modulation schemes, and the measured EVM for a -55dBm 100MS/s 64-QAM (256-QAM) signal is -31dB (-30.2dB).

Compared with prior art with a similar operating frequency range and BW [3-5] in Fig. 19.1.6, this work demonstrates higher IB linearity and sharper filtering roll-off. Moreover, it was tested and passed all the 3GPP requirements, thus making it a proven architecture for the LA-BS applications.

References:
[1] Y. -C. Lien et al., "Enhanced-Selectivity High-Linearity Low-Noise Mixer-First Receiver With Complex Pole Pair Due to Capacitive Positive Feedback," *IEEE JSSC*, vol. 53, no. 5, pp. 1348-1360, May 2018.
[2] D. J. McLaurin et al., "A Highly Reconfigurable 65nm CMOS RF-to-Bits Transceiver for Full-Band Multicarrier TDD/FDD 2G/3G/4G/5G Macro Basestations," *ISSCC*, pp. 162-163, Feb. 2018.
[3] A. N. Bhat et al., "A Baseband-Matching-Resistor Noise-Canceling Receiver With a Three-Stage Inverter-Only OpAmp for High In-Band IIP3 and Wide IF Applications," *IEEE JSSC*, vol. 56, no. 7, pp. 1994-2006, July 2021.
[4] H. Razavi et al., "A 0.4–6 GHz Receiver for Cellular and WiFi Applications," *IEEE JSSC*, vol. 57, no. 9, pp. 2640-2657, Sept. 2022.
[5] M. A. Montazerolghaem et al., " A 3dB-NF 160MHz-RF-BW Blocker-Tolerant Receiver with Third-Order Filtering for 5G NR Applications," *ISSCC*, pp. 98-99, Feb. 2021.
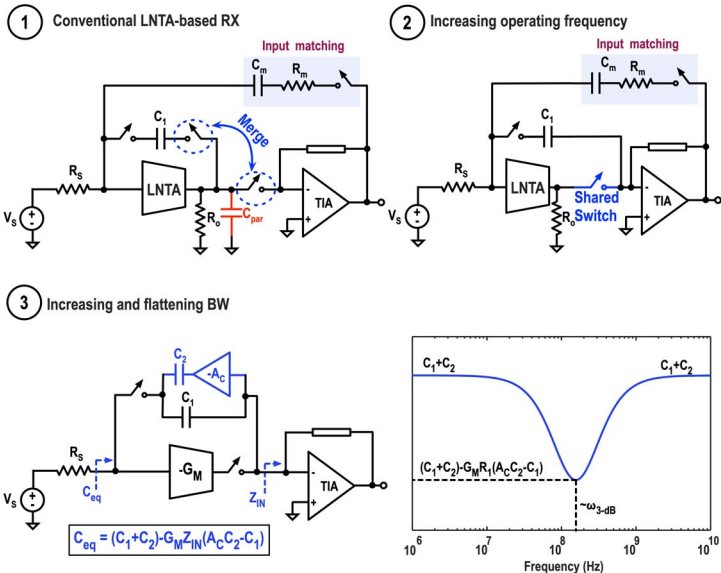
Figure 19.1.1: Proposed techniques for improving the receiver's operating frequency, bandwidth, and in-band flatness.
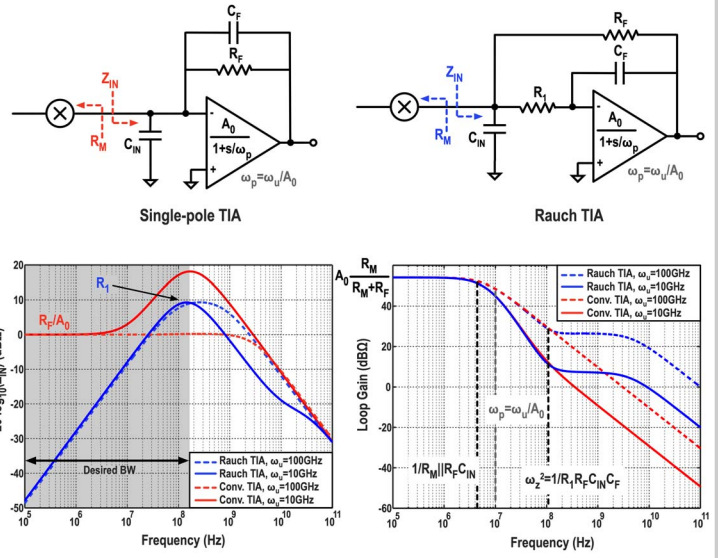

Figure 19.1.2: Comparison between the schematic, input impedance, and loop gain of the single-pole and Rauch transimpedance amplifiers adopted in the proposed RX.
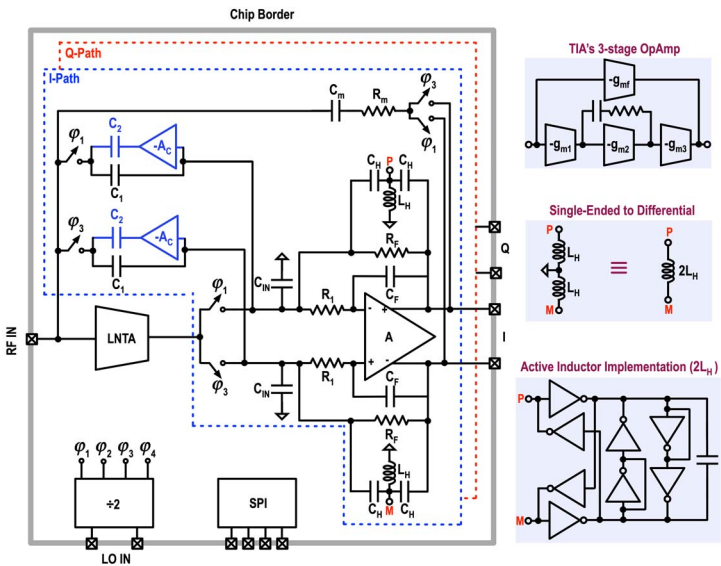

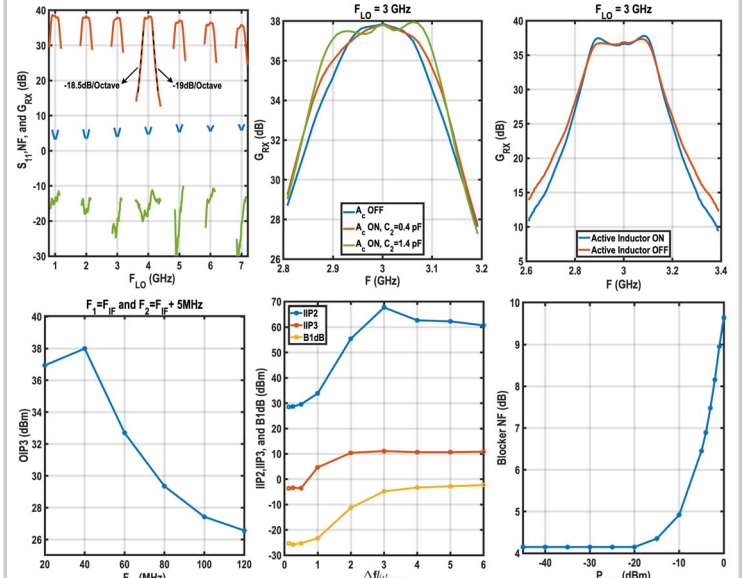Figure 19.1.3: Block diagram of the proposed receiver.

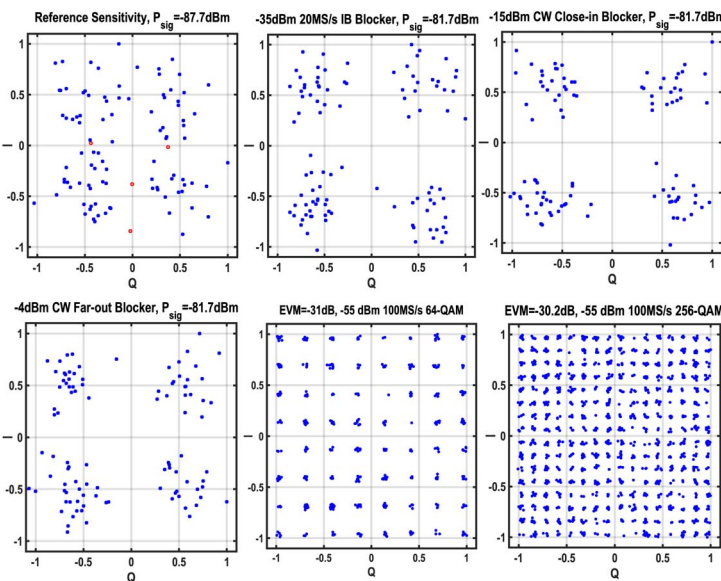Figure 19.1.4: Small- and large-signal measurement results.

Figure 19.1.5: Measured constellation diagram and EVM in different scenarios.

19

	Lien JSSC 2018 [1]	Bhat JSSC 2022 [3]	Montazerolghaem ISSCC 2021 [5]	Razavi JSSC 2022[4]	This Work
Architecture	Mixer first	Mixer first	LNTA based	LNTA based	LNTA based
Technology	45 nm SOI	22 nm SOI	40 nm	28 nm	40 nm
f_{RF} (GHz)	0.2 - 8	1 - 6	0.4 - 3.2	0.4 - 6	0.4 – 7.3
Gain (dB)	21	22.4	36	54	38
Flat BW	Yes	No	Yes	No	Yes
Single Ended Input	No	No	Yes	Yes	Yes
BW (MHz)	20	350	160	0.2 - 160	300
NF (dB)	2.3 - 7	2.5 - 5	2.7 - 3.6	2.11[†]/4.42[§]	3.2 - 5.8
0dBm Blocker NF (dB)	4.7	N/A	8.4	5.2[†]/7.4[§]	9.65
Filtering roll-off (dB/dec)	-40	-20	-55	-60	-60
IB OIP3 (dBm)	21	28.5-34.4	17	19[§]	27-38
OOB IIP3 (dBm)	39 $\Delta f/\omega_{3\text{-}dB}$ = 8	18 $\Delta f/\omega_{3\text{-}dB}$ = 5.7	10 $\Delta f/\omega_{3\text{-}dB}$ = 3	3[§] $\Delta f/\omega_{3\text{-}dB}$ = 12.5	11 $\Delta f/\omega_{3\text{-}dB}$ = 3
OOB IIP2 (dBm)	88 $\Delta f/\omega_{3\text{-}dB}$ = 8	N/A	50 $\Delta f/\omega_{3\text{-}dB}$ = 3	20[§] $\Delta f/\omega_{3\text{-}dB}$ = 12.5	67.7 $\Delta f/\omega_{3\text{-}dB}$ = 3
B1dB(dBm)	12 $\Delta f/\omega_{3\text{-}dB}$ = 4	3 $\Delta f/\omega_{3\text{-}dB}$ = 5.7	-5 $\Delta f/\omega_{3\text{-}dB}$ = 5	N/A	-4.8 $\Delta f/\omega_{3\text{-}dB}$ = 3
EVM (dB)	N/A	N/A	-26.4[¥]	-25.3[¢]	-31[œ]
Supply (V)	1.2	0.83	1.3/1.2	1	1.3
Active Area (mm²)	0.8	0.48	0.6	1.9	0.42
Power (mW)	50mW+ 30mW/GHz	172	58.5+ 17.6mW/GHz	23 - 49	100+ 13mW/GHz

†Low noise mode, § Harmonic reject mode, $ Maximum bandwidth, ¢ -57dBm 80MS/s 64-QAM, , ¥ -60dBm 140MS/s 64-QAM, œ -55dBm 100MS/s 64-QAM.

Figure 19.1.6: Performance comparison with state-of-the-art receivers operating over a wide frequency range.

Authorized licensed use limited to: TU Delft Library. Downloaded on April 18,2023 at 14:01:38 UTC from IEEE Xplore. Restrictions apply.
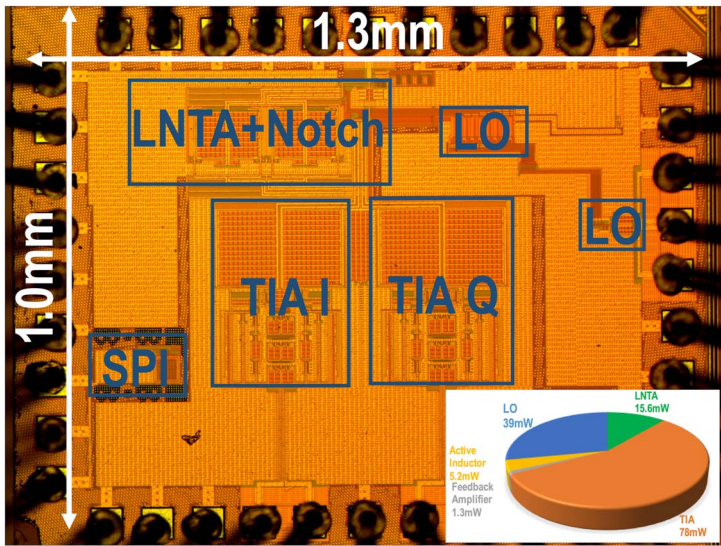
DIGEST OF TECHNICAL PAPERS • 293

Figure 19.1.7: Die micrograph and power consumption breakdown at 3GHz LO frequency.